# Three-phase fluidized bed electrochemical reactor for the scalable generation of hydrogen peroxide at enzyme compatible conditions

Michael Abt, Matthias Franzreb, Mirco Jestädt, André Tschöpe *

*Institute of Functional Interfaces, Karlsruhe Institute of Technology, Hermann-von-Helmholtz-Platz 1, 76344 Eggenstein-Leopoldshafen, Germany*

ARTICLE INFO

*Keywords:*
Electrochemical reactor
Particle electrode
Fluidized bed electrode
Co-factor generation
Oxygen reduction reaction
Electro-enzymatic

ABSTRACT

Enzymes, as green biocatalysts, open new and selective syntheses routes for more efficient and direct process steps with minimal by-products. An innovative approach is the combination of an enzymatic reaction with an electrochemical reaction to provide otherwise expensive co-factors for enzymes electrochemically. However, there is a lack of scalable reactor designs with high volume specific electrode surfaces that are required to achieve competitive space time yields for these electro-enzymatic syntheses. Here, we show for the first time a three-phase fluidized bed electrochemical reactor for co-factor generation that allows *in-situ* delivery of educts for electro-enzymatic syntheses. The performance of the fluidized bed electrode consisting of highly conductive graphite particles, was characterized for the electrochemical generation of $H_2O_2$, the co-factor for e.g. industrially relevant hydroxylation reactions applying peroxygenases, via oxygen reduction. The achieved space time yields range up to 5.15 ± 0.27 g/(L•d) for batch and 10.47 ± 0.73 g/(L•d) for continuous operation, while reaching current efficiencies of up to 57.0 ± 8.2 %. As the results were obtained at neutral pH and at low electrolyte concentrations the fluidized bed electrode is especially suitable for integrated systems combining enzymatic and electrochemical reactions in one reaction chamber. By this, we successfully developed a scalable particle electrode reactor for electro-enzymatic synthesis, which takes advantage of the excellent mixing and mass transfer properties of fluidized beds. This reactor allows for controllable co-factor generation through various factors such as pH in the counter electrode, supplied air flow, and applied potential.

## 1. Introduction

Most of the industrially relevant processes for the production of chemicals are based on fossil fuel, which results in $CO_2$ emissions that can hardly be avoided. [1,2] To reduce $CO_2$ emissions in industrial processes, the innovative field and green alternative of electro-biotechnology can be applied [3]. This field combines electrochemistry and biotechnology and enables $CO_2$ neutral synthesis of chemicals through renewable electrical energy, green biocatalysts, and sustainable resources [4]. In addition to the environmental benefits of $CO_2$ neutral synthesis of chemicals, most biocatalysts offer high selectivity and enable efficient byproduct-free synthesis [3]. Even though biocatalysts have many advantages over conventional synthesis of chemicals, pure enzymatic systems have a significant cost disadvantage. [1,2] This cost disadvantage is mainly caused by expensive co-factors such as NADPH, ATP and FAD. [1,2,5,6] However, the combination of these two fields of electrochemistry and biotechnology can reduce this drawback. In electro-enzymatic processes, the co-factor can be generated or regenerated electrochemically, which can make the synthesis process more economically attractive. [7–9].

In many industrial processes hydrogen peroxide is used as a chemical. Applications can be found in organic syntheses, water treatment and energy conversion. [10–15] Far more important for this publication, however, is the application of hydrogen peroxide as a co-factor for a variety of enzymatic processes. [16] The conventional production of hydrogen peroxide is carried out by an anthraquinone process, which consists of hydrogenations, oxidations and distillation steps for its concentration. [10,12,13,17,18] Unfortunately, this process is characterized by high energy consumption and large volumes of solvent waste. [10,12] Another promising approach is the electrochemical on-demand production of hydrogen peroxide in an electro-enzymatic process. Here, the co-factor is generated directly in the reactor, allowing accurate and precise addition of the co-factor and preventing possible inhibition of the enzyme due to excess concentration. [9,19–22] It should be noted that special conditions must be present in an electro-enzymatic process, which are characterized by a close to neutral pH, low electrolyte

* Corresponding author.
*E-mail addresses:* michael.abt@kit.edu (M. Abt), andre.tschoepe@kit.edu (A. Tschöpe).

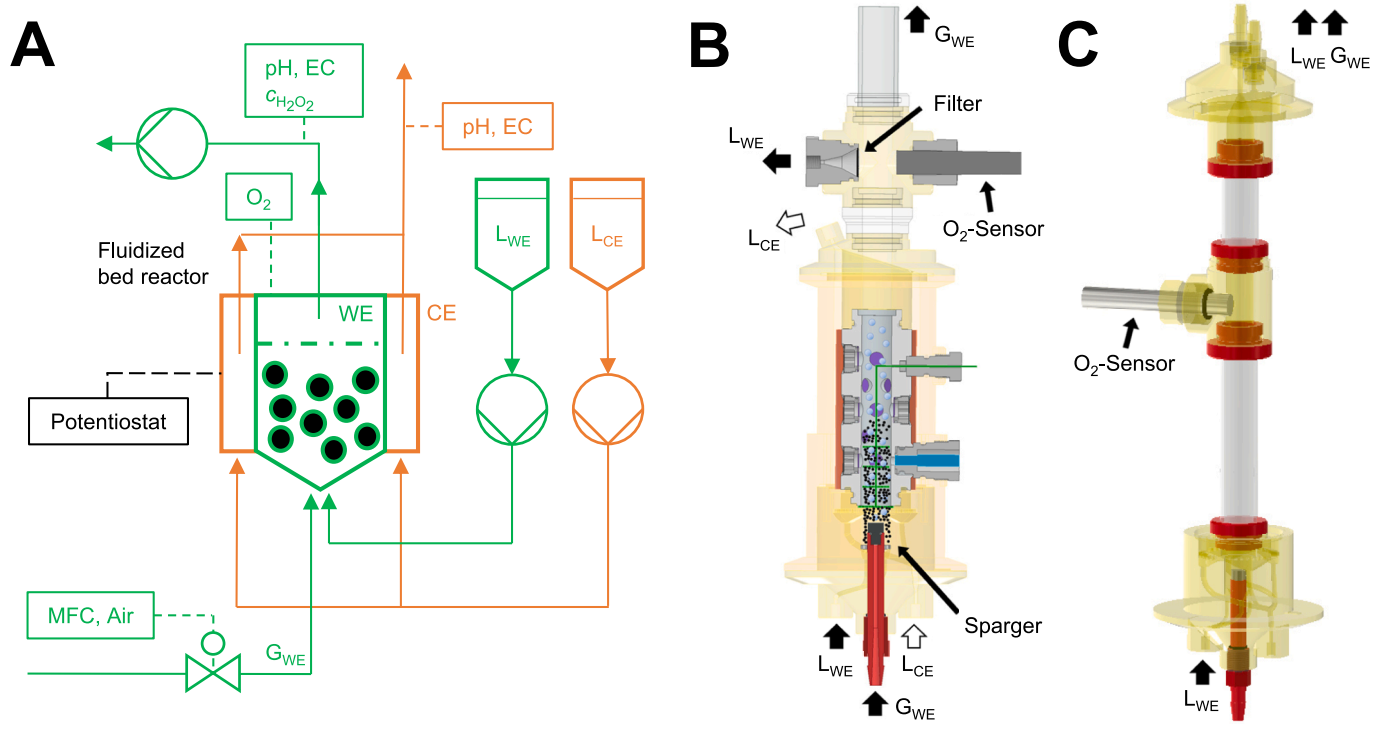


**Fig. 1.** A: Schematic illustration of the experimental setup. The working (WE, green) and counter electrode (CE, orange) chamber of the fluidized bed reactor were separately supplied with electrolyte by two piston pumps. In batch operation mode, the pumps were used to fill the reactor. In continuous operation mode, the electrolytes were pumped through the reactor and a third pump withdrew the $H_2O_2$ enriched liquid from the WE chamber. At the outlets hydrogen peroxide, pH, and electrolyte conductivity (EC) were measured. The reactor was connected to a potentiostat and a mass flow controller (MFC) fed air into the system. B: Visualization of the electrochemical reactor. The gas (G) and liquid (L) inlets for counter and working electrode are highlighted. The reactor included a sparger for gas distribution and a sensor for dissolved oxygen ($O_2$) to measure air saturation. C: Illustration of a plexiglass tube reactor, which had the dimensions of the working electrode chamber to investigate fluidization and hydrodynamic properties of the particle electrode. (For interpretation of the references to color in this figure legend, the reader is referred to the web version of this article.)

concentration and a large electrode surface with adequate current density [23,24]. The required large volume-specific surface areas of the electrodes are commonly realized by so-called 3D electrodes which consist of an interconnected 3D structure of a highly conductive material, such as a stack of metal grids or highly porous carbon foams [23]. An important type of 3D electrodes suitable for electrochemical reactions including a gaseous phase are gas diffusion electrodes (GDE). [15,23,25,26] In case of GDEs, one side of the electrode faces the gas phase and the other side faces the reaction solution. [12,13,16] Electrochemical systems applying GDEs have shown impressive mass transfer rates for the gaseous component. [13,25] Nevertheless their scale-up capability is challenging because the electrochemical reaction is not evenly distributed throughout the GDE but located within a layer, were the gas/liquid phase boundary forms. [11,27] Therefore, there exists a demand for alternative three phase 3D electrode types, which are easy to scale. A promising candidate are so-called fluidized bed particle electrodes through which a gaseous phase in the form of small bubbles can penetrate.

In general, particle electrodes offer a very large volume specific surface, which offers advantages in reaction systems with low substrate initial concentrations. [28–31] Fixed bed and fluidized bed electrodes share this advantage. Nevertheless, compared to fixed-bed electrodes, fluidized-bed electrodes are convincing in terms of their good mass- and heat transport as well as mixing properties. [32–36] Even in systems with an additional gas feed respectively in systems with a debris-containing reaction solution, the gas bubbles respectively debris can flow through the fluidized bed without being retained or the particle bed being blocked. [37] Additionally, fluidized beds show the advantage of a lower pressure drop within the particle bed at elevated flow velocities. [34,35] However, a serious disadvantage of fluidized bed electrodes is encountered in the fast decay of their electrical conductivity with increasing bed expansion. In a fluidized bed electrode, the fluidized particles repeatedly lose contact with other particles for short periods of time. [34,38–41] If this problem of contacting is not taken into account, only a small portion of the particle bed is effectively used for the electrochemical reaction. [42,43] However, it has been shown in previous publications that the problem of contacting the electrode particles can be minimized by a suitable selection of electrode particles and an intelligent design of the current source. [32,33,37,44,45].

In this work, the applicability of a fluidized bed electrode for the co-factor generation of a bioelectrochemical reaction system is evaluated for the first time. The reaction investigated is the generation of hydrogen peroxide, which is required as a co-factor for enzymes of the group of peroxygenases. In this context, the electrochemical generation of hydrogen peroxide can be achieved by oxygen reduction using the following equation [12,46]:

$$2H^+ + 2\,e^- + O_2 \rightarrow H_2O_2 \qquad (1.1)$$

In the presence of $H^+$ ions, the dissolved oxygen can be electrochemically reduced to hydrogen peroxide by means of a two-electron transfer. [12,46] In addition to the target reaction mentioned above, several competing side reactions can occur simultaneously: (1) the reduction of hydrogen peroxide to water, which occurs due to the accumulation of hydrogen peroxide at the working electrode, (2) the reduction of $H^+$ ions and dissolved oxygen to water, which is governed by a four-electron transport, and (3) the hydrogen evolution reaction, which lowers current efficiency and produces undesired hydrogen gas (equation (1.2), (1.3) and (1.4)) [10–13,46–50].

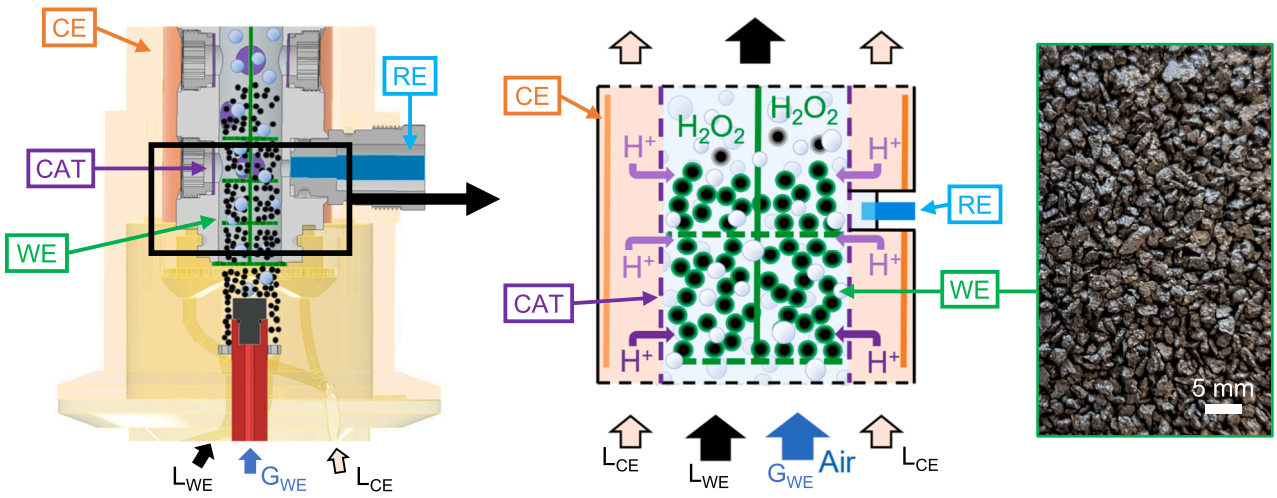


**Fig. 2.** Graphical representation of the fluidized bed reactor cross-section. In the reactor, the counter (CE) and the working electrode (WE) were separated by a cation exchange membrane (CAT). The three-electrode setup was completed by an Ag/AgCl reference electrode (RE), which was inserted from the side into the WE chamber. To distribute the current in the graphite particle working electrode a platinized four level titanium grid was placed in the center. The counter electrode consisted of a platinized titanium wire wrapped around the working electrode chamber. In the reactor concept, the WE reduced $O_2$ to $H_2O_2$ and the CAT prevented unwanted $H_2O_2$ oxidation at the CE. In contrast, the required $H^+$ for $2e^-$ reduction could transfer via the CAT from the CE to the WE, while the electrolyte in the working electrode chamber was buffered and stayed at a neutral pH in order to keep enzyme compatible conditions. The necessary oxygen was resupplied and finely distributed by an air sparger at the reactor bottom. The inlets for the air flow in the WE chamber ($G_{WE}$, Air), the electrolyte flow in the WE chamber ($L_{WE}$) and the electrolyte flow in the CE ($L_{CE}$) are indicated by arrows.

$$2\ H_2O_2 \rightarrow O_2 + 2\ H_2O \quad (1.2)$$

$$4H^+ + 4\ e^- + O_2 \rightarrow 2\ H_2O \quad (1.3)$$

$$2H^+ + 2\ e^- \rightarrow H_2 \quad (1.4)$$

It must be noted here that in order to minimize side reactions, optimal conditions must be selected for the target reaction. The reactions are influenced by the pH value, the electrolyte concentration, the applied potential between working and reference electrode, the respective overpotentials of the electrocatalyst, the reaction at the counter electrode, the oxygen supply rate, and the mass transfer. All these parameters can be optimized in a conventional electrochemical process but can only be considered to a certain degree in an electro-enzymatic system to stay within the ideal conditions of the enzymatic reaction [23].

In this work, we investigate the use of a fluidized bed electrode for the *in-situ* generation of hydrogen peroxide as a co-factor for electro-enzymatic processes in a three-phase reaction system. In addition, in order to be suitable for future electro-biotechnological processes, the reactor design and the chosen experimental conditions have been especially adapted to the requirements of enzymes.

## 2. Material and methods

### 2.1. Chemicals and electrode particles

All chemicals were of analytical grade and were used without further purification. Ultrapure water purified by a synergy water purification system (Merck Millipore, USA) was used to prepare all reaction solutions. For the fluidized bed electrode commercial graphite particles (Desulco 9018, Superior Graphite, USA) were selected and sieved to a fraction between 800 and 1200 µm. We determined the particle size distribution by a digital microscope (Keyence, Japan) and the software ImageJ. Prior to all experiments the particles were repeatedly washed with 50 % (v/v) ethanol solution and with purified water.

### 2.2. Electrochemical fluidized bed reactor

The housing for the electrochemical fluidized bed reactor was fabricated via additive manufacturing with an Objet260 Connex 3 printer using the photopolymer VeroClear of the company Stratasys (Rechovot, Israel). The reactor housing consisted of four main parts: an inner reactor chamber, an outer reactor chamber, a reactor bottom, and a reactor lid. The outer and inner reactor chamber formed a concentric, cylindrical assembly, which was based on a previous prototype design of our research group [32]. All parts were sealed by radial or axial EPDM (ethylene propylene diene terpolymer) gaskets. The fully assembled gas–liquid-solid fluidized bed reactor is shown in Fig. 1B.

#### 2.2.1. Reaction chamber

The core of the reactor was formed by a working and a counter electrode chamber separated by a membrane. An enlarged cross-section of the reactor of Fig. 1B is shown in Fig. 2 and all main elements of the reactor chamber are color-coded. The 17 mL working electrode (WE, green) chamber contained the particle electrode, which was contacted by a current distributor made of four levels of platinized titanium grid. A screw type Ag/AgCl (RE-3VT, ALS, Japan) reference electrode (RE, light blue) was used as the potential reference point in the working electrode chamber. A coiled platinized titanium wire formed the counter electrode (CE, orange) and was separated by a 130 µm PEEK reinforced (FKB-PK-130 PEEK-reinforced, Fumatech, Germany) cation exchange membrane (CAT, purple). This separation of the reaction chambers allowed to have different electrolytes in the counter and working electrode chamber.

#### 2.2.2. Reactor bottom and lid

The reactor bottom contained two separate electrolyte inlets for working and counter electrode chamber. For the air supply and a fine gas distribution in the WE, a rod with a sparger attachment made of sintered stainless steel (length: 5 mm, diameter: 8 mm, pore size: 2 µm) was installed in the center of the reactor bottom. To maintain an equal distribution of the electrolyte solution, the inlet flow was routed around the sparger rod. For this purpose, the inlet flow was divided into first two and then four symmetrically arranged flow channels. The four flow channels opened into the working chamber in four concentrically arranged inlet ports. The electrolyte flow was thus guided in an annular gap with a hydraulic diameter of 3 mm and was not expanded to the entire working chamber diameter of 15 mm until it reached the sparger. To enhance flow distribution, the annular gap was filled with 1 mm glass beads, while a filter of 6 µm mesh size was placed above the layer of glass

beads to hold back the graphite electrode particles. The liquid inlet of the counter electrode chamber followed the same design principle of four concentrical flow channels and guaranteed a good distribution of the electrolyte.

In addition to the reactor bottom, a reactor lid with a gas outlet was designed for the reactor. The goals of the design were to integrate a sensor for dissolved oxygen (Oxybase, PreSens precision sensing, Germany), to retain particles attached to gas bubbles, and to allow continuous operation. The reactor lid design added 18 mL of head space volume to the WE chamber and is shown in Fig. 1B. The reactor lid was open at the top, allowing exhaust air to escape and particles to be hold back at the gas–liquid phase boundary. The liquid outlet was placed in a side opening with a filter, thus allowing to operate the reactor continuously.

### 2.3. Experimental setup

The experimental setup is shown in the flow diagram in Fig. 1A. The electrolytes entering the counter and working electrode chamber were supplied from two reservoirs by piston pumps of an FPLC (Fast Protein Liquid Chromatography) system (Äkta purifier 100, GE Healthcare, Buckinghamshire, UK). The air flow in the reactor was controlled by a mass flow controller (FC260, Tylan General, Germany), while the pressure was regulated at 1.6 bar overpressure. The potential between working and reference electrode was applied by a potentiostat Interface 5000 from Gamry (Warmister, USA). For continuous operation, the counter and the working electrode chamber were operated in flow-through mode. The electrolyte containing the product had to be withdrawn from the working chamber by means of a separate pump. At both outlets pH, electrolyte conductivity and $H_2O_2$ concentration were measured by sampling.

### 2.4. Hydrodynamic reactor characterization

To investigate the hydrodynamics of the fluidized bed electrode, the transparent acryl glass reactor in Fig. 1C was used. The column resembles the dimensions of the working electrode which allows to transfer the determined volumetric mass transfer coefficient $k_La$ and the bed expansion $\varepsilon_S$ to the electrochemical reactor.

#### 2.4.1. Investigation of bed expansion

To evaluate the fluidization state of the particle bed electrode, the bed expansion was experimentally determined for different air flow rates. While increasing the air flow rate step by step, we measured the column volume occupied by the particle electrode. For calculation of the bed expansion, the initial volume of the particle electrode $V_{0,S}$ was compared to the volume of the fluidized state $V_S$ at a certain air flow rate in equation (2.1):

$$\varepsilon_S = V_S / V_{0,S} \tag{2.1}$$

#### 2.4.2. Determination of $k_La$ value

A dynamic approach was chosen to determine the $k_La$ value for different air flow rates in the fluidized bed reactor. Prior to each experiment, the reactor was almost completely degassed with nitrogen until an oxygen concentration of 0.5 ppm or lower was measured. The reactor was then gassed with air and the change in dissolved oxygen concentration over time $dc_{L,O_2}/dt$ was recorded. The individual runs were terminated as soon as saturation could be reached in the oxygen concentration ($c^*_{O_2}$). The measured saturation curve was used to calculate the $k_La$ value by linearizing the data via equations (2.2) and (2.3):

$$\frac{dc_{L,O_2}}{dt} = k_La \bullet (c^*_{O_2} - c_{L,O_2}) \tag{2.2}$$

$$\ln(c^*_{O_2} - c_{L,O_2}) = -k_La \bullet t \tag{2.3}$$

### 2.5. Electrochemical operation

#### 2.5.1. Electrochemical generation of $H_2O_2$

In order to be compatible for enzymatic reactions, the working electrode chamber always contained a 100 mM potassium phosphate buffer of pH 6.1. Due to the separated chambers, the conditions at the counter electrode could be varied, so that the counter electrode chamber contained 250 mM $K_2SO_4$, which was adjusted to the investigated pH values of 8.1, 6.1, 4.1 and 3.1. Prior to the experiment, these electrolytes were saturated with air and filled in the reactor. To start the electrochemical $H_2O_2$ production, the fluidized bed was expanded by air and a potential of 0.25, 0.40, 0.55 or 0.70 V vs Ag/AgCl was applied. During continuous operation, the buffer solutions were redelivered with 3 mL/min in the working electrode and 6 mL/min in the counter electrode. Besides the pH and the potential, the influence of the air flow was evaluated on the electrochemical $H_2O_2$ generation. The $k_La$ values were determined in advance and respectively the air flows corresponding to the $k_La$ values of 0.3, 0.5, 1.0 and 1.5 1/min were applied. During the experiment, samples were taken in regular intervals and the $H_2O_2$ concentration, pH and conductivity were measured. The $H_2O_2$ concentrations were determined via a Cu(II)-neocuproine based photometric $H_2O_2$ test kit (Supelco Spectroquant, Merck) at a wavelength of 445 nm by an UV–Vis photometer (Tecan Spark, Suisse). Prior to the measurement, all samples were diluted below a $H_2O_2$ concentration of 0.18 mM based on semiquantitative enzymatic test strips (Supelco MQuant, Merck).

The $H_2O_2$ production rate $\dot{q}_p$ represented the generated $H_2O_2$ concentration $c_{H_2O_2}$ per time $t$. For the calculation via equation (2.4), the $H_2O_2$ concentration within the working electrode chamber was considered after a reaction time of 15 min:

$$\dot{q}_p = \frac{c_{H_2O_2}}{t} \tag{2.4}$$

The space time yield (STY) was calculated via the mass of generated hydrogen peroxide $m_{H_2O_2}$ per time $t$ and per occupied electrode volume $V_e$ (equation (2.5)). In case of the particle electrode, the occupied electrode volume was determined based on the bed expansion at the corresponding air flow rate. For all batch experiments, the rate of $H_2O_2$ formation was determined after a reaction time of 15 min. For continuous operation, the accumulated volume for the full process duration was considered.

$$STY = m_{H_2O_2} / (V_e \bullet t) \tag{2.5}$$

#### 2.5.2. Cyclic voltammetry

Cyclic voltammetry (CV) was done to determine the operation window of the electrochemical reaction and to investigate the electrocatalytic activity of the electrodes for $O_2$ reduction. We evaluated the reactor with current feeder and after addition of the electrode particles. The working electrode contained a 100 mM potassium phosphate buffer (pH 6.1) and the counter electrode 250 mM $K_2SO_4$ at pH 3.1. Prior to every CV, the electrolyte was saturated with nitrogen or with air and the reactor was fully sealed. The scan rate was chosen to be 2 mV/s and all scans were following IUPAC convention with a scan cycle from high to low and low to high potentials.

### 2.6. Calculation of electrochemical performance indicators

All electrochemical performance indicators were determined at 15 min of a batch experiment and for the full process during continuous operation.

#### 2.6.1. Current density

The current density $j$ was calculated according to equation (2.6) by normalizing the average current $I$ with the electrode surface $A_e$ (current feeder: 17.5 $cm^2$, 4.5 g electrode particles 121.3 $cm^2$). For the estimation of the particle electrode surface, the particles were simplified as spheres.

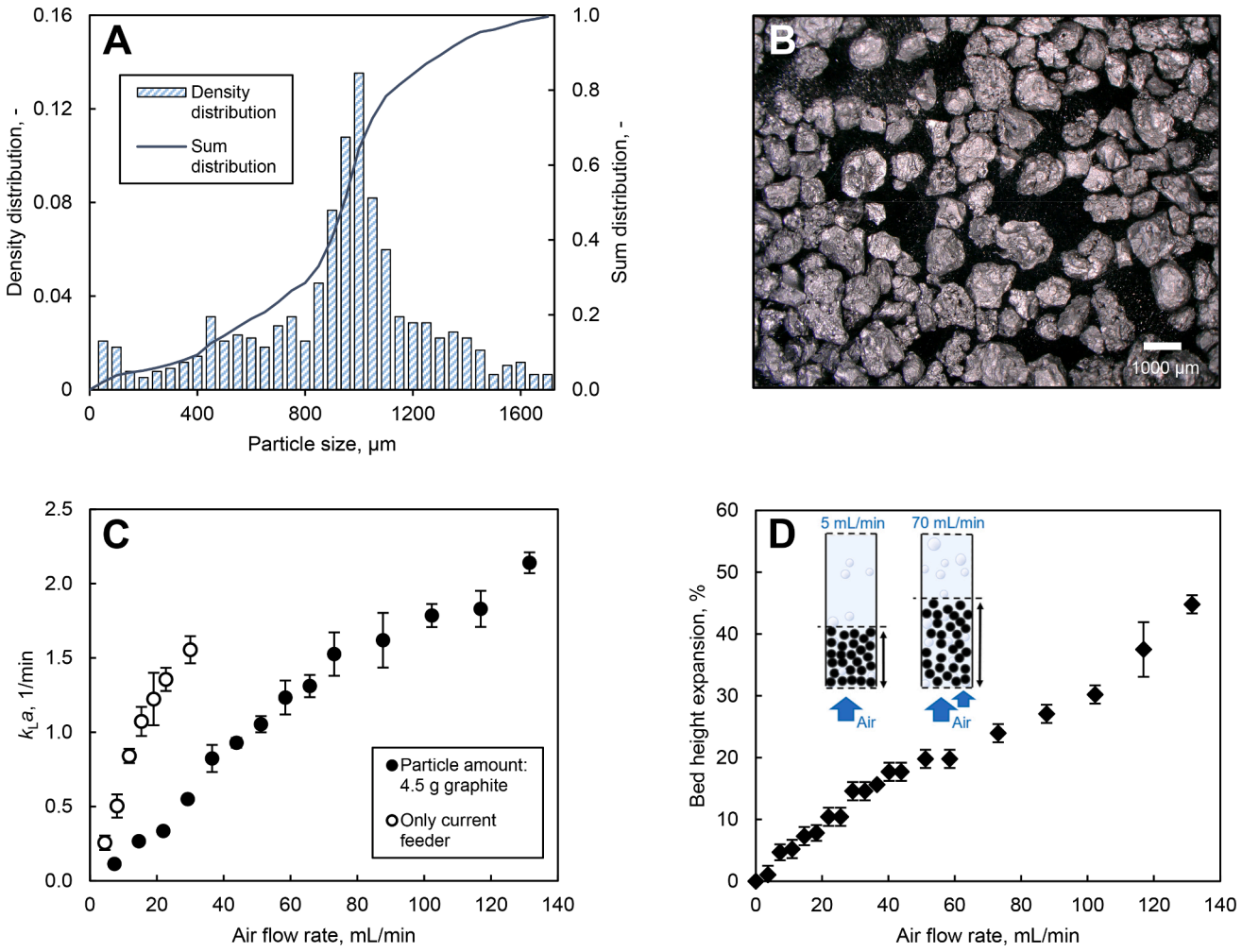


**Fig. 3.** Particle and fluidization properties of the working electrode. A: Number density and sum distribution of the graphite electrode particles. B: Microscope image of the graphite particles. C: Gas-liquid oxygen intake in the fluidized bed reactor. The volumetric mass transfer coefficient $k_La$ was determined in dependence of the air flow rate with the current feeder only and after addition of 4.5 g electrode particles. D: Relative bed height expansion when fluidizing 4.5 g of the graphite electrode particles at different air flow rates. The insets indicate the bed height expansion of the fluidized bed electrode due to the increase of air flow from 5 to 70 mL/min.

$$j = \frac{I}{A_e} \tag{2.6}$$

### 2.6.2. Current efficiency

The current efficiency $\Phi^e_{H_2O_2}$ was defined as the ratio of charge for the $H_2O_2$ generation $Q_{H_2O_2}$ and the total quantity of charge $Q_{total}$, that passed in a certain time. The charge quotient can also be described as a function of the amount of hydrogen peroxide, the number of electrons $z$ for oxygen reduction reaction to hydrogen peroxide, the Faraday's constant $F$ and the integrated total current over time (equation (2.7)). The amount of hydrogen peroxide $n_{H_2O_2}$ was determined via multiplying the $H_2O_2$ concentration by the volume during batch (35 mL) and by the accumulated volume during continuous operation.

$$\Phi^e_{H_2O_2} = \frac{Q_{H_2O_2}}{Q_{total}} = \frac{n_{H_2O_2} \bullet z \bullet F}{\int_0^t I(t)\mathrm{d}t} \tag{2.7}$$

## 3. Results and discussion

### 3.1. Properties of the fluidized bed electrode

An important aspect of the three-phase fluidized bed reactor is the particle bed electrode, which is used as the working electrode and fluidized by means of the gas phase inflow. Especially, the parameters particle size, the volumetric mass transfer coefficient of oxygen from gas to liquid phase in the presence of particles and the particle bed expansion have a prominent role in the considered system. It must be noted that these parameters influence themselves mutually and must be weighed against each other, in order to attain ideal process parameters for the reaction system. The results of the parameter investigations are shown in the Fig. 3.

Fig. 3A and B show the particle size distribution (PSD) and a microscopic image of the electrode particles. Looking at the PSD, it can be seen that the electrode particles used have a broad size distribution of approximately 400 to 1500 µm and a mean particle size of 950 µm. The microscopic images show that the electrode particles used have a shape that is not fully spherical. Depending on the size, distribution and shape of the particles, the fluidization is thus influenced. [51,52] In a three-phase fluidized bed reactor the course of particle fluidization can only be reliably determined by experiments. A special feature as well as a challenge of the described system is that the fluidization is achieved with an additional air flow into the reaction chamber. The finely dispersed air bubbles allow the electrode particles to reach an expansion state even when the pump rate of the liquid phase is set to 0, as shown in Fig. 3D. This demonstrates a nearly linear relationship of air flow to particle bed expansion in a range from 0 to 50 mL/min. Beyond the airflow of 50 mL/

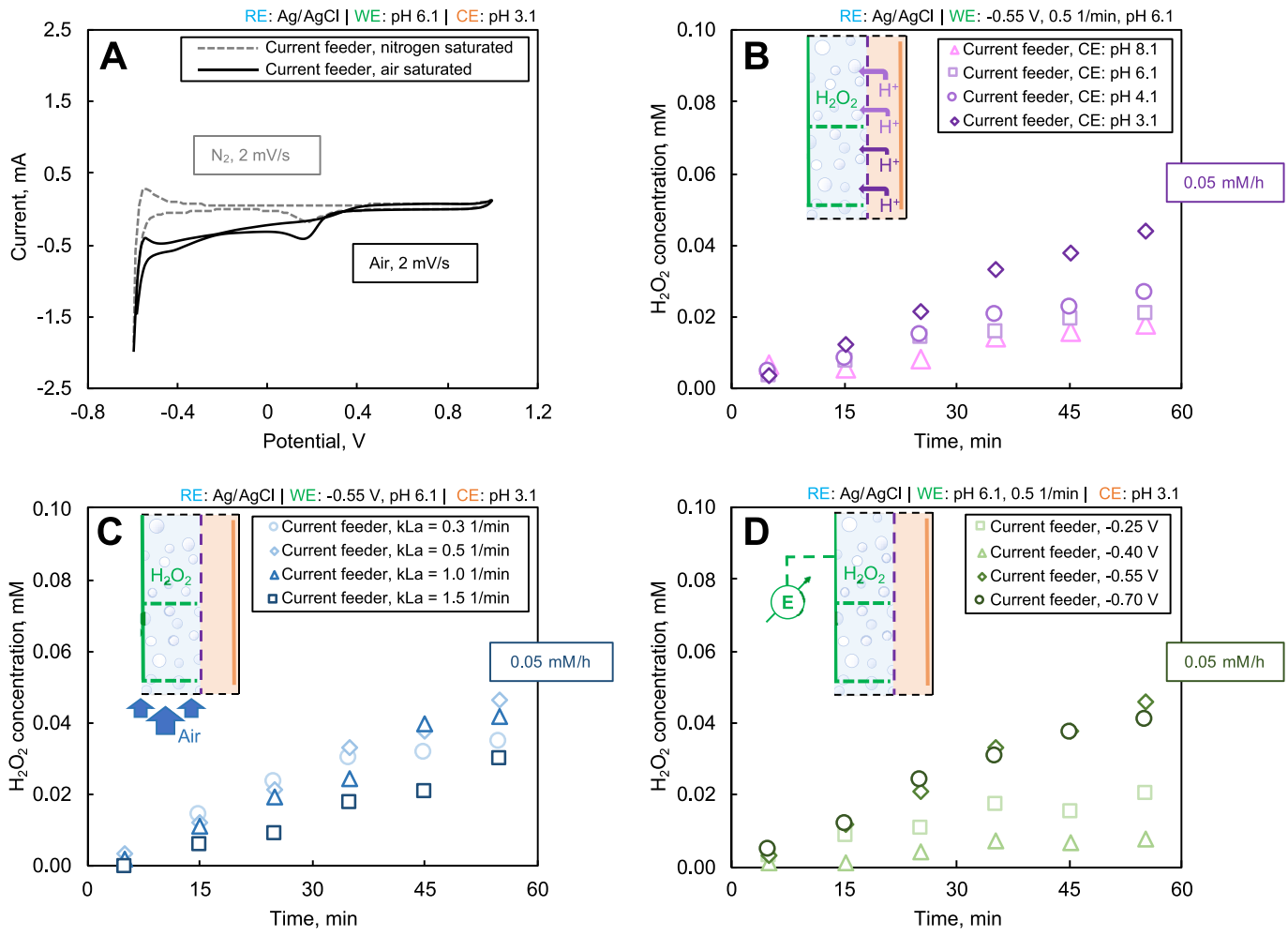


**Fig. 4.** Results of the electrochemical batch generation of $H_2O_2$ within the three-electrode reactor setup with only the platinized titanium current feeder as working electrode (WE), a platinized titanium wire coil as counter electrode (CE) and an Ag/AgCl reference electrode (RE). The electrolytes are 100 mM potassium phosphate buffer at pH 6.1 in the WE chamber and 250 mM $K_2SO_4$ in the CE chamber. A: Cyclic voltammetry of the platinized titanium current feeder in $N_2$ and air saturated buffer in the WE chamber as well as a pH value of 3.1 in the CE chamber. B: Investigation of the $H_2O_2$ generation of the current feeder at different pH values in the CE chamber at a potential of −0.55 V and a $k_La$value of 0.5 1/min. C: Investigation of the $H_2O_2$ generation of the current feeder at different $k_La$ values at a potential of −0.55 V and a pH value of 3.1 in the CE chamber. D: Investigation of the $H_2O_2$ generation of the current feeder at different potentials vs Ag/AgCl at a $k_La$ value of 0.5 1/min and a pH value of 3.1 in the CE chamber. A-D: For each experiment, the varied parameters are indicated in the inset and the legend of each illustration.

min, the particle bed expansion becomes more irregular. It should be mentioned that in previous studies it was shown that a particle bed expansion of more than 10 % is negative for the conductivity and limits the usability of the particle electrode for the electrochemical reaction process [32,42]. In this context, a particle bed expansion of 10 % can be achieved in this system with an air flow rate of 21 mL/min. In addition to the particle bed expansion, the air flow has another important role in the three-phase reaction system of the fluidized bed electrode. The air flow supplies the reaction system with an oxygen supply, which is necessary for the generation of hydrogen peroxide. Thereby, the gaseous oxygen in the air must first dissolve into the liquid phase of the system. This process can be expressed by the volumetric mass transfer coefficient $k_La$ (Fig. 3C). For comparison, the $k_La$-value was examined as a function of the air flow rate for the reaction system with and without the particle electrode. Fig. 3C shows, that higher $k_La$-values can be achieved without particle electrode even at lower air flow rates. In the particle electrode system, higher air flow rates must be set to produce similar oxygen transfer rates. This is due to the fact that the finely dispersed air bubbles agglomerate in the particle bed, which has a negative effect on mass transfer from the gas phase to the liquid phase. For the following series of experiments, although higher air flows have a negative influence on the electrical contacting of the particle electrode, oxygen transfer rates of 0.3 (19 mL/min), 0.5 (30 mL/min), 1.0 (48 mL/min) and 1.5 1/min (73 mL/min), corresponding to particle bed expansions of 8, 15, 19 and 24 %, were investigated. For the set of experiments without the particle electrode, the air flow rate was reduced, and the oxygen transfer rates were 0.3 (4 mL/min), 0.5 (8 mL/min), 1.0 (15 mL/min) and 1.5 1/min (23 mL/min).

### 3.2. *Batch $H_2O_2$ production applying only the current feeder as WE*

The platinized titanium current feeder was chosen as easily formable, conductive material to maximize the contacting of the particle electrode. The four-level mesh structure was chosen based on previous research, which showed that for larger distances from the grid, the contacting of the fluidized particles gets insufficient. [32,33,37].

The reactor without particle electrode was investigated to evaluate the influence of the platinized current feeder on the reaction system in terms of electrochemical functionality and to validate the reactor concept (Fig. 4). For this purpose, cyclic voltammetry experiments and experiments for the generation of hydrogen peroxide, varying different parameters such as the pH, the air gassing and the potential between the working and reference electrodes, were performed. In addition, these experiments aimed to serve as a reference for the electrochemical

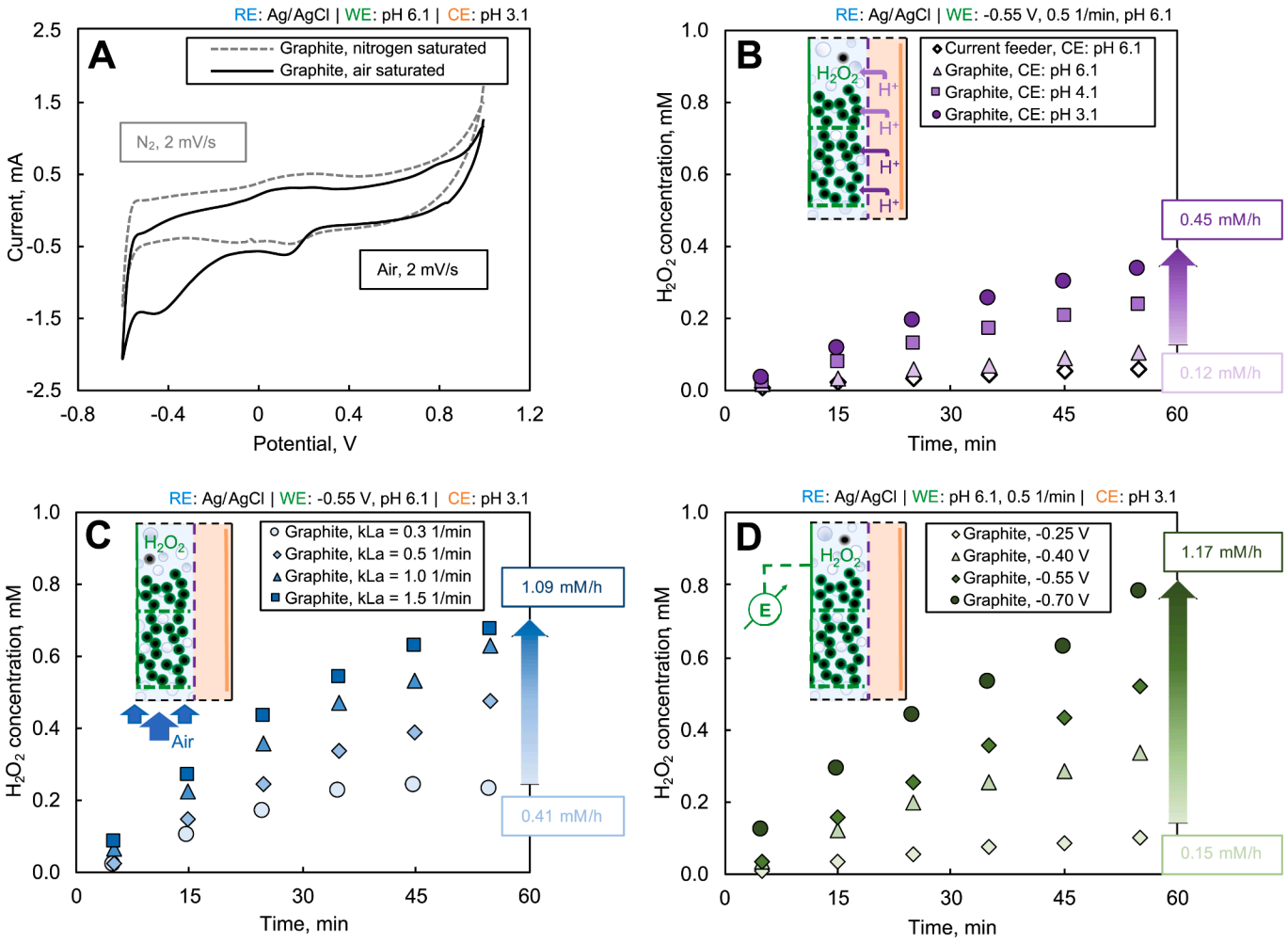


**Fig. 5.** Results of the electrochemical batch generation of $H_2O_2$ within the reactor setup with current feeder and particle electrode as working electrode (WE), a platinized titanium wire coil as counter electrode (CE) and an Ag/AgCl reference electrode (RE). The electrolytes are 100 mM potassium phosphate buffer at pH 6.1 in the WE chamber and 250 mM $K_2SO_4$ in the CE chamber. A: Cyclic voltammetry of the graphite particle electrode (4.5 g) in $N_2$ and air saturated buffer in the WE chamber as well as a pH value of 3.1 in the CE chamber. B: Batch $H_2O_2$ generation of the fluidized particle electrode at different pH values in the CE chamber at a potential of −0.55 V and a $k_La$ value of 0.5 1/min. C: Batch $H_2O_2$ generation of the fluidized particle electrode at different $k_La$ values at a potential of −0.55 V and a pH value of 3.1 in the CE chamber. D: Batch $H_2O_2$ generation of the fluidized particle electrode at different potentials vs Ag/AgCl at a $k_La$ value of 0.5 1/min and a pH value of 3.1 in the CE chamber. A-D: For each experiment, the varied parameters are indicated in the inset and the legend of each illustration.

experiments with the particle electrode.

Cyclic voltammetry experiments were conducted to determine the operation window of the current feeder potential and to find the optimal conditions for $H_2O_2$ generation (Fig. 4A). The voltammogram shows the start of the oxygen reduction at around 0.25 V during the sweep in negative direction in an air saturated solution. In comparison, a solution saturated with nitrogen shows only a minor initial peak in this region and practically no current if the potential is in the region between 0 to 0.40 V. This indicates that in the presence of oxygen a reduction is taking place and increases the current flow. However, at platinized surfaces the $4e^-$ oxygen reaction starts at a more positive onset potential than the $2e^-$ oxygen reaction, so that the formation of water is thermodynamically favored and starts at a potential of around 0.20 V already. [49,53,54] Therefore, the reduction peak observed in the CV indicates the dominance of the $4e^-$ reaction and low efficiencies of $H_2O_2$ production must be expected. For the aimed $2e^-$ reaction probably higher reduction potentials are needed. However, for the platinized surfaces water electrolysis already starts at around 0.55 V, narrowing the usable operation window of WE potential into a range where only limited $H_2O_2$ generation can be expected.

Given that the current feeder is in contact with the electrolyte, also in case of the experiments with the particle bed electrode, it is crucial to determine its influence on $H_2O_2$ generation and current consumption, even though the electrode surface of the current feeder (17.5 $cm^2$) is limited compared to the surface of the particle electrode (121.7 $cm^2$). In Fig. 4B, the $H_2O_2$ generation of the platinized current feeder is shown at different pH values in the counter electrode. The highest $H_2O_2$ production rate of 0.05 mM/h was reached at pH 3.1 in the counter electrode chamber with a current efficiency of 4.6 %. In contrary, the lowest hydrogen peroxide generation of 0.02 mM/h was observed at pH 8.1 with a current efficiency of 2.1 %. This proves the importance of the proton transfer through the CAT and the successful enhancement of transfer when the CE electrolyte is more acidic while still keeping the pH in the WE chamber around pH 6. Using a buffered system, protons can be transported by hydrogen phosphate ions which dissociate at the WE electrode due to the locally increased pH. Since the best hydrogen peroxide production rates were achieved by a pH of 3.1 in the counter electrode chamber, this condition was set for the subsequent series of experiments.

The following examination of the influence of the air flow rate (Fig. 4C) showed that the maximum hydrogen peroxide production rate (0.05 mM/h) was already reached at an $k_La$-value of 0.5 1/min. Interestingly, increasing the $k_La$ value further to 1.0 and 1.5 1/min actually reduced the $H_2O_2$ production rate. Here, the benefit of an increased

oxygen input is outweighed by the negative effect of gas bubbles isolating parts of the electrode surface.

Another parameter influencing the oxygen reduction at the current feeder is the potential between the working and the reference electrode. Looking at Fig. 4D, it is evident that with increasing the reduction potential from −0.25 V to −0.55 V, the hydrogen peroxide production undergoes a maximum of 0.05 mM/h. At the same time, however, with a potential increase to −0.70 V, no further increase in hydrogen peroxide production can be achieved. In the cyclo-voltammogram (Fig. 4A) it showed that water electrolysis starts at a voltage of −0.55 V. In view of this it is obvious that an increase of the voltage to −0.70 V will not enhance hydrogen peroxide production but will cause water electrolysis. Consequently, the current efficiency at this condition is reduced from 4.6 % to 1.8 %, while the hydrogen peroxide production rate remains the same. The full data of the $H_2O_2$ production rates, the current densities, the current efficiencies and the space time yields are listed in the SI.

In summary, this first set of experiments investigating the extend of hydrogen peroxide generation of the current feeder, demonstrated optimal conditions with respect to the pH value in the counter electrode chamber, the air flow rate and the potential range. Thereby, these data provide a first starting point for the subsequent experiments with application of a particle electrode. Also, the results show that the application of only the current feeder results in a hydrogen peroxide production rate of up to 0.05 mM/h, indicating that the electrode surface of the titanium grid is not sufficient to obtain significant production rates. In addition, it turned out that platinized titanium shows a bad selectivity towards oxygen reduction into hydrogen peroxide resulting in low current efficiencies. Therefore, in order to increase the reactor performance, a larger electrode surface area delivered by a material with higher selectivity for electrochemical hydrogen peroxide generation is needed.

### 3.3. Batch $H_2O_2$ production with a fluidized bed particle electrode

In a second set of experiments, the WE chamber of the reactor was filled with the particle electrode and the same parameter variations as described in chapter 3.2 were evaluated. Looking at the voltammogram of the air saturated solution (Fig. 5A) a similar reduction peak at around 0.25 V than in case of the CV with the current feeder only (Fig. 4A) can be observed. The fact that the height of the reduction peak did not significantly increase despite the strong increase of the theoretical electrode surface by the graphite particles is an indication, that the oxygen reduction at 0.25 V still is dominated by reactions at the platinized current feeder. Another observation is that the voltammogram in nitrogen saturated solution shows an enhanced, almost rectangular hysteresis which is caused by capacitive effects of the high electrode surface of the graphite particles [55,56]. The hysteresis is visible also in the case of the voltammogram in air saturated solution, but in the potential range between 0 to −0.40 V an additional effect becomes dominant, strongly increasing the current by about 1 mA. The additional current most likely is a result of oxygen reduction at the graphite particle electrode. Even more important, due to the high selectivity of carbon materials for the $2e^-$ reduction reaction of oxygen, the additional current compared to the experiments with only the platinized current feeder favours $H_2O_2$ generation [17,57–59]. The potential when this happens is not clearly identifiable as a peak, because the potential drop within the particle electrode results in an additional shift of the voltage when the reactions take place. The potential drop rises with increasing distance from the current feeder, ending up in a relatively broad potential range in which the oxygen reduction reaction can be observed within the voltammogram. Investigating pure graphite, the potential for the start of water electrolysis would also be strongly shifted to more negative potential [56,60,61]. However, in our system the platinized current feeder is present and therefore the occurrence of water electrolysis remains at about −0.55 V, still limiting the usable operation window of the electrode potential. This indicates that the potential range between −0.40 to −0.55 V is the ideal operation window with the least side reactions in our reaction system.

Looking at the influence of the pH value in the counter electrode chamber on the electrochemical generation of hydrogen peroxide in the buffered working electrode chamber, the system with the particle electrode (Fig. 5B) shows similarities to the system with the current feeder only (Fig. 4B). Again, the decrease of the pH value of 6.1 to 3.1 resulted in a strong increase in the $H_2O_2$ production rate from 0.12 to 0.45 mM/h as well as a higher current efficiency of 5.8 % to 29.1 %. The water electrolysis occurring in the counter electrode chamber should stoichiometrically supply the required hydrogen ions needed for the production of hydrogen peroxide. Though, with respect to the low production rate of 0.12 mM/h, the redelivery of $H^+$ via the membrane seems limited at pH 6.1 in the counter electrode chamber. Reducing the pH in the counter electrode chamber in order to make this region more acidic, however, can promote the availability of $H^+$ at the cation exchange membrane. The consumed hydrogen ions are thus replenished by the $H^+$-transfer across the cation exchange membrane resulting in a higher $H_2O_2$ generation. It should be mentioned, that the exact mechanism is still unclear in neutral pH conditions, which are present in the working electrode chamber. [62] Since the best hydrogen peroxide production rates in our system were obtained at a pH of 3.1 in the counter electrode chamber, these conditions were set for all subsequent experiments.

In the previous investigations without a particle electrode, it was found that higher air gassing rates had no or even a detrimental effect on the hydrogen peroxide production rate (Fig. 4C). A different behavior is observed in case of the reactor with a particle electrode in the working electrode chamber (Fig. 5C). By increasing the air flow rate, corresponding to an increase in the oxygen mass transfer from 0.3 to 1.5 1/min, the hydrogen peroxide production rate was substantially improved from 0.41 to 1.09 mM/h. Furthermore, a higher air flow rate has also a positive effect on the current efficiency of the system. A possible explanation is the strong mixing in case of high air flow rates, moving the generated hydrogen peroxide away from the electrocatalyst, i.e. the electrode surface. As a result, the generated hydrogen peroxide does not undergo any further reduction reaction [63]. Additionally, the stronger mixing improves the oxygen transfer from the gas to the liquid phase as well as the transfer of the $H^+$-ions penetrating the CAT. Interestingly, the particle electrode still seems to have sufficient electrical contacting due to the design of the current feeder. Even at a particle bed expansion of 24 % ($k_La$ = 1.5 1/min) the hydrogen peroxide production rate is improved. In former work of our group and others, an expansion of the fluidized bed of about 10 % was considered to be optimal, in order to maintain a good electrical contacting of the fluidized bed electrode [32,42].

Finally, the WE potential as one of the key parameters of the electrochemical reaction, was studied for the reactor including the particle electrode. As expected, the production rate of hydrogen peroxide increases with rising reduction potential and reaches its highest value of 1.17 mM/h at a potential of −0.70 V (Fig. 5D). However, in contrast to the experiments with the current feeder only, the potential step from −0.40 V to −0.70 V resulted in a strong increase in $H_2O_2$ production. The explanation for this difference is given by the potential drop within the particle electrode. Because of this potential drop, applying a potential of −0.40 V to the current feeder means that a fraction of the particle bed is operating at an electrode potential of −0.30 V or even lower, depending on the distance of the particles from the current feeder. Increase the current feeder potential to −0.70 V guarantees that also particle fractions having a larger distance operate at reduction potentials which enable them to take place in the aimed oxygen reduction reaction. However, increasing the potential to −0.70 V comes at the price that water electrolysis occurs at the current feeder and thus, the current efficiency is reduced. At a potential of −0.70 V, a current efficiency of 28.2 % could be achieved, while a potential of −0.40 V resulted in current efficiencies of up to 39.0 %. An overview of the key

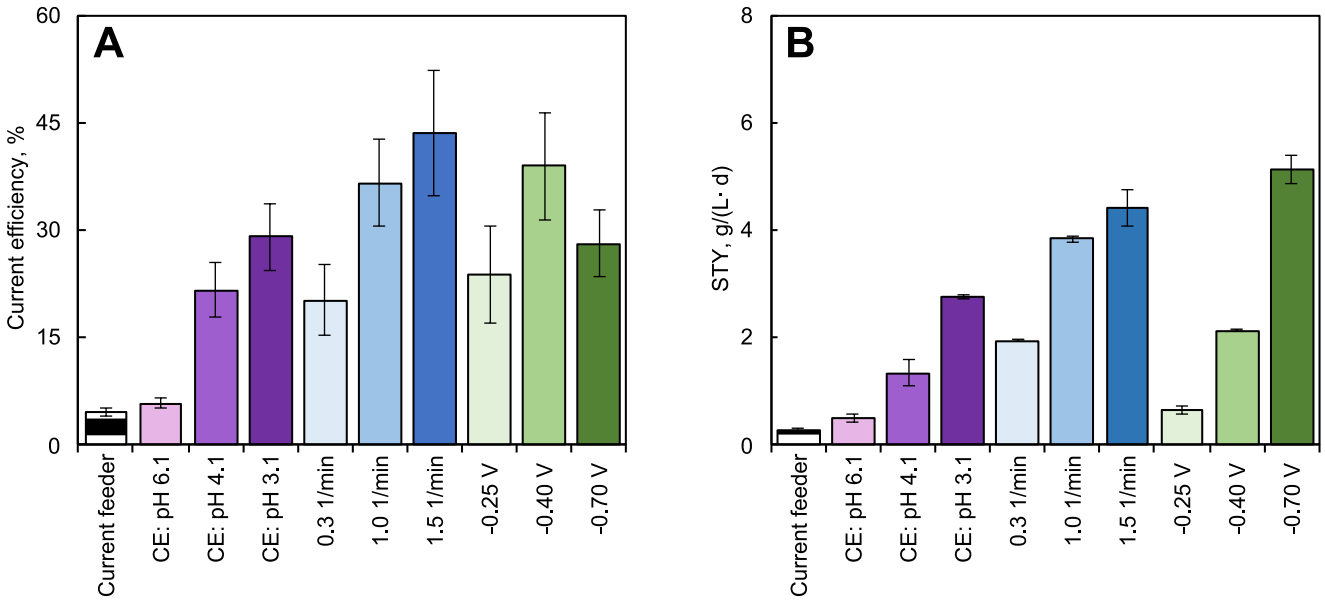


**Fig. 6.** Key performance indicators determined for the batch $H_2O_2$ generation with graphite electrode particles of Fig. 5. For comparison, one of the experiments with the platinized current feeder of Fig. 4 is listed. The current density (A) and the current efficiency (B) are shown at 15 min of the experiments. For each experiment, the varied parameter is shown. All other process conditions are −0.55 V, 0.5 1/min, pH 3.1 in the CE chamber and pH 6.1 in the WE chamber, if not specifically varied in the experiment.

**Table 1**
Summary of the performance indicators determined for the batch $H_2O_2$ generation with graphite particle electrode (Fig. 5 and Fig. 6). For comparison, one of the experiments with the platinized current feeder of Fig. 4 is listed. The electrolytes are 100 mM potassium phosphate buffer at pH 6.1 in the WE chamber and 250 mM $K_2SO_4$ in the CE chamber. The current density, the current efficiency, the $H_2O_2$ production rate, and the space time yield are shown at 15 min of the experiments.

| Electrode | Parameters: Potential, V | pH in CE | $k_La$, 1/min | Current density, µA/cm² | $\Phi^e_{H_2O_2}$, % | $H_2O_2$-rate, mM/h | STY, g/(L•d) |
|---|---|---|---|---|---|---|---|
| Current feeder, batch | 0.55 | 3.1 | 0.5 | 115 ± 12 | 4.6 ± 0.5 | 0.05 ± 0.01 | 0.28 ± 0.04 |
| Graphite particles, batch | 0.55 | 6.1 | 0.5 | 31 ± 4 | 5.8 ± 0.7 | 0.12 ± 0.01 | 0.51 ± 0.07 |
| Graphite particles, batch | 0.55 | 4.1 | 0.5 | –22 ± 4 | 21.7 ± 3.8 | 0.31 ± 0.04 | 1.35 ± 0.24 |
| Graphite particles, batch | 0.55 | 3.1 | 0.5 | 34 ± 5 | 29.1 ± 4.6 | 0.63 ± 0.01 | 2.76 ± 0.05 |
| Graphite particles, batch | 0.55 | 3.1 | 0.3 | 30 ± 8 | 20.3 ± 4.9 | 0.41 ± 0.01 | 1.94 ± 0.02 |
| Graphite particles, batch | 0.55 | 3.1 | 1.0 | 37 ± 6 | 36.7 ± 6.1 | 0.90 ± 0.02 | 3.84 ± 0.07 |
| Graphite particles, batch | 0.55 | 3.1 | 1.5 | 38 ± 8 | 43.7 ± 8.8 | 1.09 ± 0.08 | 4.44 ± 0.34 |
| Graphite particles, batch | 0.25 | 3.1 | 0.5 | 9 ± 3 | 23.9 ± 6.7 | 0.15 ± 0.02 | 0.65 ± 0.07 |
| Graphite particles, batch | 0.40 | 3.1 | 0.5 | 19 ± 4 | 39.0 ± 7.5 | 0.49 ± 0.01 | 2.14 ± 0.02 |
| Graphite particles, batch | 0.70 | 3.1 | 0.5 | 64 ± 11 | 28.2 ± 4.7 | 1.17 ± 0.06 | 5.15 ± 0.27 |

performance indicators (current efficiency and STY) extracted from the experiments applying a particle electrode is shown in Fig. 6. The values of current efficiency and STY are listed and summarized together with the current density and $H_2O_2$ production rate in Table 1. For comparison, the performance indicators of the experiment showing the highest $H_2O_2$ production rate for the reactor with current feeder only is also included. The results show that due to limited electrode area and the early occurrence of water electrolysis, the current feeder of the present system is not ideal and offers potential for further improvement. Nevertheless, the achieved STY is close to the best ones reported in literature for other reactor designs for *in-situ* $H_2O_2$ generation. Using an enzymatic cascade for $H_2O_2$ generation Ni et al. achieved an estimated STY of 5.63 g/(L•d) [64]. A similar STY of 4.90 g/(L•d) could be obtained by a plasma-driven process for $H_2O_2$, but the highest STY of 7.34 g/(L•d) for enzyme compatible *in-situ* $H_2O_2$ generation reported so far results also from an electrochemical process applying a GDE as WE [65,66].

### 3.4. Continuous $H_2O_2$ generation with a fluidized bed electrode

After finding optimum conditions for batch *in*-situ electrochemical $H_2O_2$ generation under enzyme compatible conditions, in a last step we modified the system in order to allow continuous operation. The batch reactor approach already offered three options to control the electrochemical co-factor generation, without changing pH or electrolyte concentration in the working electrode chamber. As it takes some time to change the pH in the counter electrode chamber, the air flow rate and the potential are chosen as promising options to control the $H_2O_2$-generation during a continuous process.

The continuous $H_2O_2$ production was investigated with an electrolyte flow rate of 3 mL/min, therefore exchanging the volume of the WE chamber (35 mL) approximately every 12 min. To keep the pH in the counter electrode chamber constant, the respective electrolyte was exchanged approximately every 15 min by a flow rate of 6 mL/min (Fig. 7B and D). In the first set of experiments, the influence of different potentials of 0.40, 0.55 and 0.70 V on the continuous electrochemical generation of hydrogen peroxide was investigated. When applying the different potentials, once again a clear correlation between the potential and $H_2O_2$-generation could be observed. The reasons for this behavior have already been discussed in the previous section. A new aspect of the continuous system is the adjustment of an equilibrium between the generation of hydrogen peroxide and its outflow from the reaction system. Such an equilibrium can be identified for all potentials after a running time of the experiment of approx. 40 min. Hereby, a

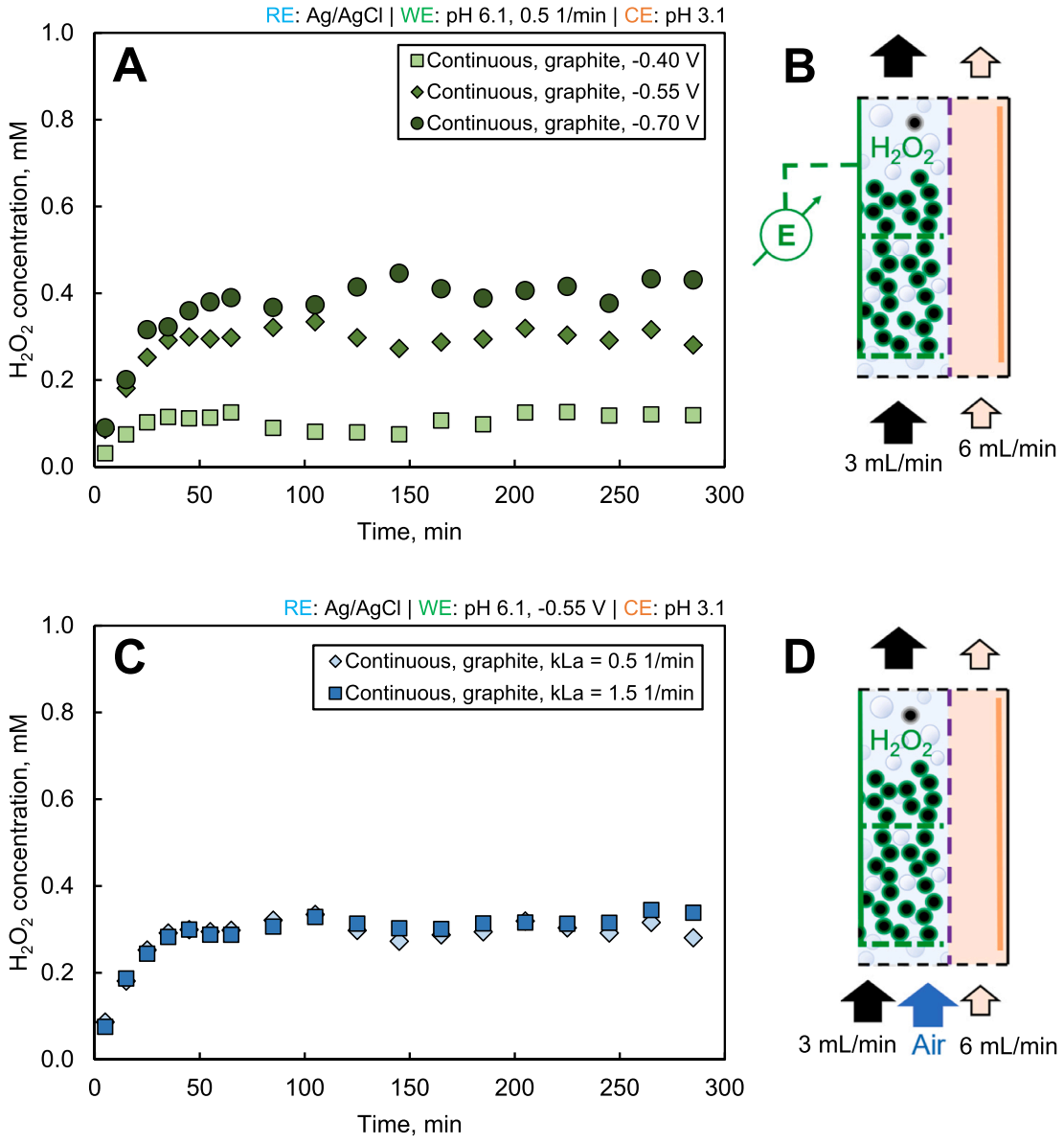


**Fig. 7.** Results of the electrochemical continuous generation of $H_2O_2$ within the reactor setup with current feeder and particle electrode as WE. A: Continuous $H_2O_2$ generation with the graphite particle electrode at different potentials vs Ag/AgCl. B: Illustration of the continuous generation at different potentials with 3 mL/min electrolyte flow in WE and 6 mL/min electrolyte flow in CE. C: Continuous $H_2O_2$ generation with the graphite particle electrode at different air flow rates. D: Illustration of the continuous generation at different air flows with 3 mL/min electrolyte flow in WE and 6 mL/min electrolyte flow in CE.

continuous effluent concentrations of hydrogen peroxide of 0.10, 0.28, and 0.37 mM could be achieved at a potential of 0.40, 0.55, and 0.70 V, respectively (Fig. 7A.). Comparing these results with the results of the batch experiments, it can be seen that the STY for the potentials of 0.40 and 0.55 V have improved by a factor of four (compare Table 1). Within the process time of 300 min, STY of 3.05 g/(L•d) at 0.40 V and of 8.48 g/(L•d) at 0.55 V were reached, while the highest space time yield of 10.47 g/(L•d) was observed at a potential of 0.70 V. Therefore, the STY at 0.55 V and especially at 0.70 V for *in-situ* electrochemical $H_2O_2$ generation under enzyme compatible conditions even exceed the one reported by Horst et al [65]. The production rate can be adjusted by the potential to match the requirements of an enzymatic reaction consuming hydrogen peroxide as co-factor. A good match of the production rate is essential, because excess hydrogen peroxide production will quickly result in enzyme inhibition by the co-factor. Another positive effect of switching from batch to continuous operation is the improvement of current efficiency. Comparing the current efficiency of the continuous process with the batch process at a potential of 0.55 V shows an increase from 29.1 to 50.9 %. One effect contributing to this improvement in STY and current efficiency is that the continuous supply of buffer near maximum air saturation provides more oxygen in addition to the oxygen supply by air sparging. Especially in the lower section of the reactor near the inlet, the additional supply results in higher oxygen saturations and allows a higher $H_2O_2$ generation than in batch mode. Another effect contributing to this improvement, is given by the fact that in continuous operation the hydrogen peroxide concentration in the particle bed region close to the inlet is also kept at a very low level due to the supply of new buffer solution, while in batch operation the hydrogen peroxide concentration constantly increases in all sections of the particle bed. Because hydrogen peroxide is prone to be further reduced to water when getting into contact with the WE, its presence in higher concentration is detrimental to the current efficiency and explains the improvement during continuous operation compared to the batch process. It should also be mentioned here that the

**Table 2**
Summary of the performance indicators determined for the continuous $H_2O_2$ generation with graphite electrode particles. The current density, the current efficiency, the $H_2O_2$-concentration, and the space time yield are listed for the full process duration of 300 min.

| Electrode | Parameters: Potential, V | pH in CE | $k_La$, 1/min | Current density, μA/cm$^2$ | $\Phi^e_{H_2O_2}$, % | $H_2O_2$-conc., mM | STY, g/(L•d) |
|---|---|---|---|---|---|---|---|
| Graphite, continuous | 0.40 | 3.1 | 0.5 | 17 ± 2 | 51.1 ± 6.9 | 0.10 ± 0.02 | 3.05 ± 0.26 |
| Graphite, continuous | 0.55 | 3.1 | 0.5 | 47 ± 9 | 50.9 ± 10.3 | 0.28 ± 0.06 | 8.48 ± 0.23 |
| Graphite, continuous | 0.70 | 3.1 | 0.5 | 74 ± 14 | 44.0 ± 8.1 | 0.37 ± 0.08 | 10.47 ± 0.73 |
| Graphite, continuous | 0.55 | 3.1 | 1.5 | 46 ± 7 | 57.0 ± 8.2 | 0.29 ± 0.06 | 7.85 ± 0.35 |

additional fluid flow has no effect on the fluidization of the fluidized bed electrode, since the minimum fluidization rate of the electrode particles without air sparging is much higher. Nevertheless, gas bubbles are more easily transported outside of the fluidized bed in case of the continuous operation, reducing the effect of blocking parts of the particle bed by sticking gas bubbles. These observations are confirmed by the increase in current density from 36 μA/cm$^2$ to 47 μA/cm$^2$, comparing the batch with the continuous process. Above all, the achieved current efficiencies are in accordance with carbon materials in literature, which are listed between 26.5 and 75.7 % at neutral pH conditions [62].

In the last set of experiments, the air flow rate was investigated as an option to further increase the $H_2O_2$ generation without the downside of lower current efficiencies, as it was already shown in batch operation experiments. In Fig. 7C the $k_La$ -values of 0.5 1/min and 1.5 1/min at a potential of 0.55 V were examined for the continuous operation process. In contrast to the batch process (Fig. 5C), the higher air flow rate does not lead to a higher production rate, and a constant hydrogen peroxide concentration of 0.29 mM is established in the effluent after approximately 40 min. On the one hand, the higher air flow rate in addition to the electrolyte flow, the fluidized bed expands further, which causes poorer electrical conductivity of the electrode particles. On the other hand, the more turbulent regime enhances the mass transfer to the electrode surface and transports the product away to avert further reduction of $H_2O_2$ [63]. These two effects seem to balance out and nearly equal current densities of 47 μA/cm$^2$ respectively 46 μA/cm$^2$ are observed at an oxygen mass transfer of 0.5 1/min respectively 1.5 1/min. Interestingly, while not improving the production rate, the higher air flow rate improves the current efficiency up to 57.0 %.

Overall, the continuous operation showed higher space time yields and improved current efficiencies compared to the batch process. The correlation of $H_2O_2$ generation and potential allows to control and to adapt the process to the rate of an enzymatic reaction in an electro-enzymatic system. If the aim is to maximize the current efficiency, the optimum set of parameters are 0.55 V, $k_La = 1.5$ 1/min and pH 3.1 in the counter electrode, resulting in a current efficiency of 57.0 % and a space time yield of 8.48 g/(L•d) (Table 2). If a higher hydrogen peroxide generation is preferred, the reactor should be operated at 0.70 V at a space time yield of 10.47 g/(L•d).

## 4. Summary and conclusions

In this study, we developed a novel three-phase fluidized bed reactor for the electro-enzymatic co-factor generation that allows to introduce educts for the enzymatic respectively electrochemical reaction during batch and continuous operation. The reactor performance was examined for the generation of $H_2O_2$, a co-factor required for enzymes of the group of peroxygenases. A design applying separated chambers for the counter and working electrode allowed to keep the WE chamber conditions in an enzyme compatible neutral pH range and at low electrolyte concentrations while offering the freedom to optimize the electrolyte properties in the counter electrode chamber. The required $H^+$ ions for the reduction of oxygen to hydrogen peroxide were transferred via a cation exchange membrane from counter to working electrode chamber and the oxygen was supplied via an air sparger at the bottom of the WE chamber. It was found, that the $H_2O_2$ generation at the graphite particle electrode was influenced by the pH-value in the counter electrode chamber, by the air flow rate and by the applied potential between working and reference electrode. In the case of batch operation, a maximum space time yield of 5.15 g/(L•d) was achieved, while fluidizing the particle electrode by an air flow. During continuous operation of the fluidized bed reactor, a fluid flow was additionally applied in the counter and working electrode chamber. Here the $H_2O_2$ generation was further improved to 10.47 g/(L•d) and optimized towards a current efficiency of up to 57.0 %. In future, the material of the current feeder should be replaced by a graphite-based system, because the platinized current feeder turned out to have unfavorable selectivity regarding the aimed 2e$^-$ reduction reaction of oxygen forming hydrogen peroxide and the unwanted 4e$^-$ reduction reaction of oxygen forming water. In contrast to traditional fuel cells and common electrolyzers, relying on a numbering up, the reactor based on a particle electrode shows promising scale up opportunities of the unit itself, thus strongly simplifying the scale-up design. Especially, during electro-enzymatic processes, the adequate current density of < 100 μA/cm$^2$ due to the large electrode surface will be exceptional beneficial. Together with the good mass transfer and mixing properties of a fluidized bed, the particle electrode enables homogenous and controllable co-factor generation for optimized electro-enzymatic processes with less enzyme inhibition by overdosing.

## Declaration of Competing Interest

The authors declare that they have no known competing financial interests or personal relationships that could have appeared to influence the work reported in this paper.

## Data availability

Data will be made available on request.

## Acknowledgements

This work was performed within the project “Bioelectrochemical and engineering fundamentals to establish electro-biotechnology for biosynthesis - Power to value-added products (eBiotech)” funded by the Deutsche Forschungsgemeinschaft (DFG) - project number 445807856.

## References

[1] R. Barin, D. Biria, S. Rashid-Nadimi, M.A. Asadollahi, Enzymatic CO2 reduction to formate by formate dehydrogenase from Candida boidinii coupling with direct electrochemical regeneration of NADH, J. CO2 Util. 28 (2018) 117–125, https://doi.org/10.1016/j.jcou.2018.09.020.
[2] R. Barin, D. Biria, S. Rashid-Nadimi, M.A. Asadollahi, Investigating the enzymatic CO2 reduction to formate with electrochemical NADH regeneration in batch and semi-continuous operations, Chem. Eng. Process. - Process Intesif. 140 (2019) 78–84, https://doi.org/10.1016/j.cep.2019.04.020.
[3] R. Wu, C. Ma, Z. Zhu, Enzymatic electrosynthesis as an emerging electrochemical synthesis platform, Curr. Opin. Electrochem. 19 (2020) 1–7, https://doi.org/10.1016/j.coelec.2019.08.004.

[4] R.A. Rincón, C. Lau, K.E. Garcia, P. Atanassov, Flow-through 3D biofuel cell anode for NAD+-dependent enzymes, Electrochim. Acta 56 (2011) 2503–2509, https://doi.org/10.1016/j.electacta.2010.11.041.

[5] S.Z. Çekiç, D. Holtmann, G. Güven, K.-M. Mangold, U. Schwaneberg, J. Schrader, Mediated electron transfer with P450cin, Electrochem. Commun. 12 (2010) 1547–1550, https://doi.org/10.1016/j.elecom.2010.08.030.

[6] A. Manjón, J.M. Obón, P. Casanova, V.M. Fernández, J.L. Ilborra, Increased activity of glucose dehydrogenase co-immobilized with a redox mediator in a bioreactor with electrochemical NAD+ regeneration, Biotechnol. Lett 24 (2002) 1227–1232, https://doi.org/10.1023/A:1016270820734.

[7] C. Cadoux, R.D. Milton, Recent Enzymatic Electrochemistry for Reductive Reactions, ChemElectroChem 7 (2020) 1974–1986, https://doi.org/10.1002/celc.202000282.

[8] K. Délécouls-Servat, R. Basséguy, A. Bergel, Membrane electrochemical reactor (MER): application to NADH regeneration for ADH-catalysed synthesis, Chem. Eng. Sci. 57 (2002) 4633–4642, https://doi.org/10.1016/S0009-2509(02)00393-7.

[9] D. Holtmann, T. Krieg, L. Getrey, J. Schrader, Electroenzymatic process to overcome enzyme instabilities, Catal. Commun. 51 (2014) 82–85, https://doi.org/10.1016/j.catcom.2014.03.033.

[10] J. Chen, N. Li, L. Zhao, Three-dimensional electrode microbial fuel cell for hydrogen peroxide synthesis coupled to wastewater treatment, J. Power Sources 254 (2014) 316–322, https://doi.org/10.1016/j.jpowsour.2013.12.114.

[11] J.I. Colades, M.D.G. de Luna, M.F.N. Secondes, C.-P. Huang, Electrochemical in-situ hydrogen peroxide generation in a packed-bed reactor for Fenton oxidation of p-nitrophenol in aqueous solution, Process Saf. Environ. Prot. 123 (2019) 161–168, https://doi.org/10.1016/j.psep.2018.10.014.

[12] H. Li, E. Quispe-Cardenas, S. Yang, L. Yin, Y. Yang, Electrosynthesis of 20 g/L H2O2 from Air, ACS ES T Eng. 2 (2022) 242–250, https://doi.org/10.1021/acsestengg.1c00366.

[13] N. Li, J. An, L. Zhou, T. Li, J. Li, C. Feng, X. Wang, A novel carbon black graphite hybrid air-cathode for efficient hydrogen peroxide production in bioelectrochemical systems, J. Power Sources 306 (2016) 495–502, https://doi.org/10.1016/j.jpowsour.2015.12.078.

[14] M. Panizza, G. Cerisola, Electrochemical generation of H2O2 in low ionic strength media on gas diffusion cathode fed with air, Electrochim. Acta 54 (2008) 876–878, https://doi.org/10.1016/j.electacta.2008.07.063.

[15] J.F. Pérez, J. Llanos, C. Sáez, C. López, P. Cañizares, M.A. Rodrigo, Electrochemical jet-cell for the in-situ generation of hydrogen peroxide, Electrochem. Commun. 71 (2016) 65–68, https://doi.org/10.1016/j.elecom.2016.08.007.

[16] S. Bormann, M.M.C.H. van Schie, T.P. de Almeida, W. Zhang, M. Stöckl, R. Ulber, F. Hollmann, D. Holtmann, H2O2 Production at Low Overpotentials for Electroenzymatic Halogenation Reactions, ChemSusChem 12 (2019) 4759–4763, https://doi.org/10.1002/cssc.201902326.

[17] J. An, Y. Feng, Q. Zhao, X. Wang, J. Liu, N. Li, Electrosynthesis of H2O2 through a two-electron oxygen reduction reaction by carbon based catalysts: From mechanism, catalyst design to electrode fabrication, Environ. Sci. Ecotechnol. 11 (2022), 100170, https://doi.org/10.1016/j.ese.2022.100170.

[18] Y. Jiang, P. Ni, C. Chen, Y. Lu, P. Yang, B. Kong, A. Fisher, X. Wang, Selective Electrochemical H 2 O 2 Production through Two-Electron Oxygen Electrochemistry, Adv. Energy Mater. 8 (2018) 1801909, https://doi.org/10.1002/aenm.201801909.

[19] S. Lütz, K. Vuorilehto, A. Liese, Process development for the electroenzymatic synthesis of (R)-methylphenylsulfoxide by use of a 3-dimensional electrode, Biotechnol. Bioeng. 98 (2007) 525–534, https://doi.org/10.1002/bit.21434.

[20] G.V. Sayoga, V.S. Bueschler, H. Beisch, D. Holtmann, A.-P. Zeng, B. Fiedler, D. Ohde, A. Liese, Application of the all-in-one electrode for in situ H2O2 generation in hydroxylation catalyzed by unspecific peroxygenase from Agrocybe aegerita, Mol. Catal. 547 (2023), 113325, https://doi.org/10.1016/j.mcat.2023.113325.

[21] C. Kohlmann, S. Lütz, Electroenzymatic Synthesis of Chiral Sulfoxides, Eng. Life Sci. 6 (2006) 170–174, https://doi.org/10.1002/elsc.200620907.

[22] T. Krieg, S. Hüttmann, K.-M. Mangold, J. Schrader, D. Holtmann, Gas diffusion electrode as novel reaction system for an electro-enzymatic process with chloroperoxidase, Green Chem. 13 (2011) 2686, https://doi.org/10.1039/c1gc15391a.

[23] T. Krieg, A. Sydow, U. Schröder, J. Schrader, D. Holtmann, Reactor concepts for bioelectrochemical syntheses and energy conversion, Trends Biotechnol. 32 (2014) 645–655, https://doi.org/10.1016/j.tibtech.2014.10.004.

[24] F. Harnisch, D. Holtmann (Eds.), Bioelectrosynthesis, Springer International Publishing, Cham, 2019.

[25] M. Stöckl, T. Lange, P. Izadi, S. Bolat, N. Teetz, F. Harnisch, D. Holtmann, Application of gas diffusion electrodes in bioeconomy: An update, Biotechnol. Bioeng. 120 (2023) 1465–1477, https://doi.org/10.1002/bit.28383.

[26] A.E.W. Horst, K.-M. Mangold, D. Holtmann, Application of gas diffusion electrodes in bioelectrochemical syntheses and energy conversion, Biotechnol. Bioeng. 113 (2016) 260–267, https://doi.org/10.1002/bit.25698.

[27] Lorenz M. Baumgartner, Christel I. Koopman, Antoni Forner-Cuenca, and David A. Vermaas, Narrow Pressure Stability Window of Gas Diffusion Electrodes Limits the Scale-Up of CO2 Electrolyzers.

[28] H. Li, H. Yang, J. Cheng, C. Hu, Z. Yang, C. Wu, Three-dimensional particle electrode system treatment of organic wastewater: A general review based on patents, J. Clean. Prod. 308 (2021), 127324, https://doi.org/10.1016/j.jclepro.2021.127324.

[29] J. Rodrigo Quejigo, S. Tejedor-Sanz, A. Esteve-Núñez, F. Harnisch, Bed electrodes in microbial electrochemistry: setup, operation and characterization, ChemTexts 5 (2019), https://doi.org/10.1007/s40828-019-0078-3.

[30] J. Cheng, H. Yang, H. Li, C. Hu, X. Yu, R. Li, Reaction mechanism of Ni-coated Cu composite powder prepared by liquid-solid fluidized bed 3D electrodes, Chem. Eng. J. 428 (2022), 132529, https://doi.org/10.1016/j.cej.2021.132529.

[31] B. Korth, N. Pous, R. Hönig, P. Haus, F.B. Corrêa, U. Da Nunes Rocha, S. Puig, F. Harnisch, Electrochemical and Microbial Dissection of Electrified Biotrickling Filters, Front. Microbiol. 13 (2022), 869474, https://doi.org/10.3389/fmicb.2022.869474.

[32] A. Tschöpe, M. Wyrwoll, M. Schneider, K. Mandel, M. Franzreb, A magnetically induced fluidized-bed reactor for intensification of electrochemical reactions, Chem. Eng. J. 385 (2020), 123845, https://doi.org/10.1016/j.cej.2019.123845.

[33] A. Tschöpe, S. Heikenwälder, M. Schneider, K. Mandel, M. Franzreb, Electrical conductivity of magnetically stabilized fluidized-bed electrodes – Chronoamperometric and impedance studies, Chem. Eng. J. 396 (2020), 125326, https://doi.org/10.1016/j.cej.2020.125326.

[34] J.N. Hiddleston, A.F. Douglas, Current/potential relationships and potential distribution in fluidized bed electrodes, Electrochim. Acta 15 (1970) 431–443, https://doi.org/10.1016/0013-4686(70)87003-7.

[35] T. Berent, I. Fells, R. Mason, Fluidized Bed Fuel Cell Electrodes, Nature 223 (1969) 1054–1055, https://doi.org/10.1038/2231054a0.

[36] J. Rodrigo Quejigo, S. Tejedor-Sanz, A. Esteve-Núñez, F. Harnisch, Bed electrodes in microbial electrochemistry: setup, operation and characterization, ChemTexts 5 5 (1) (2019), https://doi.org/10.1007/s40828-019-0078-3.

[37] A. Tschöpe, M. Franzreb, Influence of non-conducting suspended solids onto the efficiency of electrochemical reactors using fluidized bed electrodes, Chem. Eng. J. 424 (2021), 130322, https://doi.org/10.1016/j.cej.2021.130322.

[38] B.J. Sabacky, J.W. Evans, The electrical conductivity of fluidized bed electrodes—its significance and some experimental measurements, Metall. Trans. B 8 (1977) 5–13, https://doi.org/10.1007/BF02656345.

[39] G. Kreysa, S. Pionteck, E. Heitz, Comparative investigations of packed and fluidized bed electrodes with non-conducting and conducting particles, J. Appl. Electrochem. 5 (1975) 305–312, https://doi.org/10.1007/BF00608794.

[40] K. Kazdobin, N. Shvab, S. Tsapakh, Scaling-up of fluidized-bed electrochemical reactors, Chem. Eng. J. 79 (2000) 203–209, https://doi.org/10.1016/S1385-8947(00)00211-4.

[41] M. Fleischmann, J.W. Oldfield, L. Tennakoon, Fluidized bed electrodes Part IV. Electrodeposition of Copper in a Fluidized Bed of Copper-Coated Spheres, J. Appl. Electrochem. 1 (1971) 103–112, https://doi.org/10.1007/BF01111857.

[42] M. Fleischmann, J.W. Oldfield, Fluidised bed electrodes, J. Electroanal. Chem. Interfacial Electrochem. 29 (1971) 211–230, https://doi.org/10.1016/S0022-0728(71)80084-0.

[43] M. Fleischmann, J.W. Oldfield, Fluidised bed electrodes, J. Electroanal. Chem. Interfacial Electrochem. 29 (1971) 231–240, https://doi.org/10.1016/S0022-0728(71)80085-2.

[44] M. Klaiber, A. Tschöpe, K. Cu, I. Waibel, S. Heißler, M. Franzreb, J. Lahann, Multifunctional Core-Shell Particle Electrodes for Application in Fluidized Bed Reactors, ACS Appl. Eng. Mater. 1 (2023) 325–333, https://doi.org/10.1021/acsaenm.2c00072.

[45] J.R. Quejigo, B. Korth, A. Kuchenbuch, F. Harnisch, Redox Potential Heterogeneity in Fixed-Bed Electrodes Leads to Microbial Stratification and Inhomogeneous Performance, ChemSusChem 14 (2021) 1155–1165, https://doi.org/10.1002/cssc.202002611.

[46] E.M. Milner, K. Scott, I.M. Head, T. Curtis, E.H. Yu, Evaluation of porous carbon felt as an aerobic biocathode support in terms of hydrogen peroxide, J. Power Sources 356 (2017) 459–466, https://doi.org/10.1016/j.jpowsour.2017.03.079.

[47] T. Muddemann, D.R. Haupt, M. Sievers, U. Kunz, Improved Operating Parameters for Hydrogen Peroxide-Generating Gas Diffusion Electrodes, Chem. Ing. Tech. 92 (2020) 505–512, https://doi.org/10.1002/cite.201900137.

[48] C. Xia, Y. Xia, P. Zhu, L. Fan, H. Wang, Direct electrosynthesis of pure aqueous H2O2 solutions up to 20% by weight using a solid electrolyte, Science 366 (2019) 226–231, https://doi.org/10.1126/science.aay1844.

[49] E. Jung, H. Shin, W. Hooch Antink, Y.-E. Sung, T. Hyeon, Recent Advances in Electrochemical Oxygen Reduction to H 2 O 2 Catalyst and Cell Design, ACS Energy Lett. 5 (2020) 1881–1892, https://doi.org/10.1021/acsenergylett.0c00812.

[50] S.C. Perry, D. Pangotra, L. Vieira, L.-I. Csepei, V. Sieber, L. Wang, C. Ponce de León, F.C. Walsh, Electrochemical synthesis of hydrogen peroxide from water and oxygen, Nat. Rev. Chem. 3 (2019) 442–458, https://doi.org/10.1038/s41570-019-0110-6.

[51] J. Werther Ullmann's Encyclopedia of Industrial Chemistry Wiley-VCH Verlag GmbH & Co. KGaA Weinheim, Germany.

[52] K. Hertwig L. Martens C. Hamel Chemische Verfahrenstechnik: Berechnung Auslegung und Betrieb chemischer Reaktoren third. Auflage 2018 De Gruyter Berlin, Boston.

[53] S. Siahrostami, A. Verdaguer-Casadevall, M. Karamad, D. Deiana, P. Malacrida, B. Wickman, M. Escudero-Escribano, E.A. Paoli, R. Frydendal, T.W. Hansen, I. Chorkendorff, I.E.L.S. Stephens, J. Rossmeisl, Enabling direct H2O2 production through rational electrocatalyst design, Nat. Mater. 12 (2013) 1137–1143, https://doi.org/10.1038/NMAT3795.

[54] I. Katsounaros, W.B. Schneider, J.C. Meier, U. Benedikt, P.U. Biedermann, A. A. Auer, K.J.J. Mayrhofer, Hydrogen peroxide electrochemistry on platinum: towards understanding the oxygen reduction reaction mechanism, PCCP 14 (2012) 7384–7391, https://doi.org/10.1039/c2cp40616k.

[55] C. Kim, K.S. Yang, Electrochemical properties of carbon nanofiber web as an electrode for supercapacitor prepared by electrospinning, Appl. Phys. Lett. 83 (6) (2003) 1216–1218.

[56] D.S.K. Rajaguru, K.P. Vidanapathirana, K.S. Perera, Dependence of capacitive properties of an EDLC on exfoliation time of graphite electrodes, J. Mater. Sci. Mater. Electron. 32 (2021) 17580–17587, https://doi.org/10.1007/s10854-021-06291-w.

[57] Y. Wang, G.I.N. Waterhouse, L. Shang, T. Zhang, Electrocatalytic Oxygen Reduction to Hydrogen Peroxide: From Homogeneous to Heterogeneous Electrocatalysis, Adv. Energy Mater. 11 (2021) 2003323, https://doi.org/10.1002/aenm.202003323.

[58] W. Zhou, X. Meng, J. Gao, A.N. Alshawabkeh, Hydrogen peroxide generation from O2 electroreduction for environmental remediation: A state-of-the-art review, Chemosphere 225 (2019) 588–607, https://doi.org/10.1016/j.chemosphere.2019.03.042.

[59] Y. Zhou, G. Chen, J. Zhang, A review of advanced metal-free carbon catalysts for oxygen reduction reactions towards the selective generation of hydrogen peroxide, J. Mater. Chem. A 8 (2020) 20849–20869, https://doi.org/10.1039/D0TA07900F.

[60] F.E. Senftle, J.R. Grant, F.P. Senftle, Low-voltage DC/AC electrolysis of water using porous graphite electrodes, Electrochim. Acta 55 (2010) 5148–5153, https://doi.org/10.1016/j.electacta.2010.04.022.

[61] E. Peralta, R. Natividad, G. Roa, R. Marin, R. Romero, P. Thelma, A comparative study on the electrochemical production of H2O2 between BDD and graphite cathodes, Sustainable Environ. Res. (2013).

[62] Y. Pang, H. Xie, Y. Sun, M.-M. Titirici, G.-L. Chai, Electrochemical oxygen reduction for H 2 O 2 production: catalysts, pH effects and mechanisms, J. Mater. Chem. A 8 (2020) 24996–25016, https://doi.org/10.1039/D0TA09122G.

[63] S.C. Perry, S. Mavrikis, L. Wang, C. Ponce de León, Future perspectives for the advancement of electrochemical hydrogen peroxide production, Curr. Opin. Electrochem. 30 (2021), 100792, https://doi.org/10.1016/j.coelec.2021.100792.

[64] Y. Ni, E. Fernández-Fueyo, A. Gomez Baraibar, R. Ullrich, M. Hofrichter, H. Yanase, M. Alcalde, W.J.H. van Berkel, F. Hollmann, Peroxygenase-Catalyzed Oxyfunctionalization Reactions Promoted by the Complete Oxidation of Methanol, Angew. Chem. Int. Ed. Engl. 55 (2016) 798–801, https://doi.org/10.1002/anie.201507881.

[65] A. Horst, S. Bormann, J. Meyer, M. Steinhagen, R. Ludwig, A. Drews, M. Ansorge-Schumacher, D. Holtmann, Electro-enzymatic hydroxylation of ethylbenzene by the evolved unspecific peroxygenase of Agrocybe aegerita, J. Mol. Catal. B Enzym. 133 (2016) S137–S142, https://doi.org/10.1016/j.molcatb.2016.12.008.

[66] A. Yayci, Á.G. Baraibar, M. Krewing, E.F. Fueyo, F. Hollmann, M. Alcalde, R. Kourist, J.E. Bandow, Plasma-Driven in Situ Production of Hydrogen Peroxide for Biocatalysis, ChemSusChem 13 (2020) 2072–2079, https://doi.org/10.1002/cssc.201903438.